Astronomy & Astrophysics manuscript no. skymaps-with-depletion-01
August 27, 2014
© ESO 2014

Modeled IBEX/INCA skymaps including the keV-ENA source extinction in the outer heliosphere

M. Siewert and H.-J. Fahr

Argelander Institut für Astronomie der Universität Bonn, Abteilung f. Astrophysik und Extraterrestrische Forschung, Auf dem Huegel 71, 53121 Bonn (Germany)

Preprint online version: August 27, 2014

ABSTRACT

Understanding the outer heliospheric interface is a major challenge, especially in the light of recent observations by the IBEX and Voyager missions. We present further details on a new required theoretical correction that has been identified as substantial in a recent paper, the so-called source depletion effect. These results complement and expand earlier calculations of transit-time delays by presenting global skymaps of Energetic Neutral Atoms (ENAs) calculated with the depletion correction, comparing them with skymaps calculated without these corrections. Our results demonstrate that the depletion correction is critical for interpreting IBEX-High ENA fluxes generated in the inner heliosheath, and that any attempt to reconstruct the shape of the heliospheric boundary needs to include the depletion correction, unless arriving at considerably erroneous results.

Key words. Shock waves – Plasmas – Solar wind – Sun: heliosphere

arXiv:1408.6082v1 [astro-ph.SR] 26 Aug 2014

1. Introduction

In the past 10 years, new observations by the two Voyager spacecraft (Fisk 2005; Jokipii 2008; Webber & McDonald 2013) and the IBEX mission (McComas et al. 2009, 2012b,a) have generated renewed interest on the size and structure of the heliospheric boundary regions. Particularly ENA (energetic neutral atoms) skymaps, as produced by the IBEX mission, provide a line-of-sight integrated intensity that, on the basis of present understanding, turned out unexpectedly difficult to interpret (McComas et al. 2014); in fact, even the spatial region in the outer heliosphere where the observed ENA fluxes are mainly generated remains unclear till now.

One additional irritation in interpreting ENA data is introduced by the INCA/CASSINI instrument, a detector observing a structure in the global ENA fluxes between 5 and 50 keV, i.e. beyond the upper energy limit accessible to IBEX, that is topologically similar to the IBEX ribbon (Krimigis et al. 2009), however with two subtle differences. First, the INCA ENA data presents a closed ring-like region of enhanced ENA fluxes, while IBEX observes a region of enhanced ENA production that does not close upon iself. The second main difference between the observations made by both missions is the orientation of the feature; the INCA ring does not perfectly match the placement of the IBEX ribbon. Because of these differences, there is no consensus on whether both detectors are observing the same ENA source regions.

Aiming to derive a quantitative criterion that might allow to differentiate between individual models, we have recently identified a needed new correction to the calculations (Siewert et al. 2014) that was seemingly absent from all previous calculations. In the context of ENA production and observation, there are two nontrivial corrections related to the removal of particles from an initial distribution function that need to be understood for modeling and interpretation of ENA flux data. The first contribution was studied by Heerikhuisen et al. (2008) who calculated removal of ENAs along the line-of-sight between the source region and the detector. ENAs have a mean free path of o(100 AU) with respect to reionisation processes in the inner heliosphere, and therefore, a significant fraction of ENAs generated in the heliospheric boundary regions will not reach the detector.

In this study, we calculate for the first time a quantitative estimate of the other important removal process involved in the ENA production. In our model, we consider energetic protons that have been accelerated as pick-up ions at the solar wind termination shock (TS), while downstream of the TS, in the inner heliosheath, there are no additional heating processes operating, i.e. there are no further sources of energetic protons. Therefore, keV-ENA production along the plasma flow lines in the inner heliosheath will automatically break down when the initial resources of keV-energetic proton "fuel" have been extinguished, which limits relevant line-of-sight contributions to lengths of about 100 AU. In Siewert et al. (2014), we have calculated source depletion factors along a few selected lines-of-sight; in this publication, we extend these calculations to full global sky maps and compare the results to earlier calculations where the depletion correction was missing (Fahr et al. 2011; Siewert et al. 2012, 2013).

2. ENA skymaps with and without the depletion correction

In the following, we will not repeat many details of the calculation of the line-of-sight integral for the resulting fluxes, the plasma flowline profile and related problems, which have been discussed earlier in great detail by e.g. Siewert et al. (2013).

In this study, we calculate ENA skymaps according to the known relation (Lee et al. 2009)

$$\Phi_{ENA}(v_{obs}, \alpha, \delta) = \int_{r_0}^{r_1} dr \cdot j_p(E_{ENA}, \boldsymbol{r}) \sigma_{ex}(v_{rel}) n_H, \qquad (1)$$

where σ_{ex} is the charge exchange crossection, $n_H \simeq 0.1\,\mathrm{cm}^{-3}$ is the local interstellar hydrogen density, and $j_p(E_{ENA}, \boldsymbol{r})$ is the

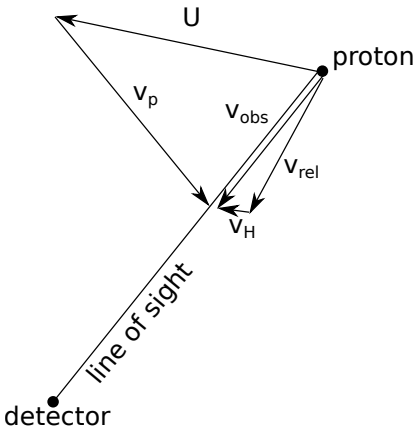

Fig. 1: Velocity vectors appearing in the ENA charge exchange problem.

source flux of energetic protons at a point $\boldsymbol{r}$. The parameters v_{ENA} and E_{ENA} denote the energy and velocity of the ions undergoing charge exchange in the rest frame convected along with the plasma flow, which is related to the ENA velocities in the observers rest frame (v_{obs}) by the relation

$$\boldsymbol{v}_{obs} = \boldsymbol{v}_{ENA} + \boldsymbol{U}, \tag{2}$$

where $\boldsymbol{U}$ is the bulk velocity of the plasma along the flowline and $\boldsymbol{v}_{obs} \parallel \boldsymbol{r}_{line-of-sight}$. Obviously, due to the presence of curved streamlines in the outer heliosheath, this relation introduces a nonlinear nontrivial correction to the flow of energetic protons. Finally, there is the relative velocity v_{rel} between the energetic plasma proton and the cold hydrogen undergoing charge exchange, for which the most general definition is given by

$$\boldsymbol{v}_{rel} = \boldsymbol{v}_p + \boldsymbol{U} - \boldsymbol{v}_H. \tag{3}$$

In the outer heliosphere, and for keV-energetic protons, one finds typical values of $v_p > U \gg v_H$, i.e. it is possible to adopt the simplification:

$$v_{rel} \simeq v_p + U \simeq v_p. \tag{4}$$

In this following study, we make use of the first approximation, where U is the projection of $\boldsymbol{U}$ on $\boldsymbol{v}_p$. We also need to mention that we are working in a pitchangle-isotropic limit, i.e. where the ion distribution function does not generate any significant anisotropy while moving along the streamlines. Depending on the energy behaviour of the charge exchange cross section and the individual velocities involved in the production process (see Fig. 1), this may not be the case when the source plasma is propagating along the flowlines; in this study, we ignore details related to pitchangle-anisotropic terms during this transport.

Finally, the differential plasma flow $j_p(E_{ena})$ appearing in Eq. 1 is defined by (see e.g. Lee et al. 2009)

$$j(E) = \frac{2}{m^2} E f(E) = v f(v) v^2 \frac{dv}{dE} = \frac{1}{m} f(v) v^2. \tag{5}$$

Now, we need to introduce a factor for the source depletion described in the introduction. Therefore, we introduce an additional factor describing the modification of the source proton distribution function,

$$f(v) \rightarrow f_0(v) \cdot \epsilon(\phi, \theta, r, v), \tag{6}$$

where $0 < \epsilon \leq 1$, and f_0 is the distribution function on the immediate downstream side of the termination shock, i.e. before energetic protons are removed by charge exchange. To calculate this parameter, one has to integrate the following differential equation along a streamline from the TS ($\epsilon = 1$, $s_0 = 0$) to the point of interest $s = s(\phi, \theta, r)$ along a line of sight:

$$U \frac{d\epsilon(v,s)}{ds} = -n_H v_{rel} \sigma_{ex}(v_{rel}) \epsilon(s), \tag{7}$$

where ds is the line element on the curved streamline. In principle, a more detailed and complicated transport equation is required, including terms for proton sources and energy diffusion; however, in the energy region between 1 and 10 keV, these other terms can be safely ignored.

A formal solution of this differential equation is given by

$$\epsilon(v,s) = n_H \int_{s_0}^{s} \frac{v_{rel}}{U} \sigma(v_{rel}) ds'. \tag{8}$$

Now, it follows from Eq. 4 that a full solution of this equation requires detailed knowledge of the plasma flow velocity field $\boldsymbol{U}(\phi, \theta, r)$ in the outer heliosphere, which must be extracted from analytical or numerical model calculations. Unfortunately, most numerical models do not provide this information in an easily accessible way, so we apply instead the analytical model by (Fahr & Fichtner 1991),

$$\boldsymbol{U} = -\boldsymbol{\nabla}_{\boldsymbol{r}} \Phi(\boldsymbol{r}), \tag{9}$$

where the velocity field is obtained from the spatial gradient of a corresponding velocity potential Φ. Even though it is possible to calculate the velocity field analytically, the resulting expressions are very lengthy and unintuitive, and therefore, we prefer to evaluate this gradient numerically.

Finally, we need to use a model for the TS geometry. We apply a description where the TS surface has an ellipsoidal form with two identical short and one longer semi major axes (as described in e.g. Scherer & Fahr 2009), where the numerical eccentricity $\varepsilon = \sqrt{1 - b^2/a^2}$ is used to characterise the deviation from a perfectly spherical shock (i.e. $\varepsilon = 0$). Figure 2 easily demonstrates that the ENA skymaps exhibit a significantly different behaviour depending on whether the depletion correction is used or not. The ring feature that can be identified as related to the IBEX ribbon emerges in considerably different regions, and analysing ENA line-of-sight data clearly requires a good handling of the depletion process.

3. Depletion maps

Next, we separate the depletion correction from the rest of the line-of-sight integral by introducing the effective depletion factor $\overline{\epsilon}$, by rewriting Eq. 1 in the form

$$\begin{aligned} \Phi_{ENA}(v_{obs}, \alpha, \delta) &= \int_{r_0}^{r_1} dr \cdot j_p(E_{ENA}) \epsilon(\phi, \theta, r) \sigma_{ex}(v_{ENA}) n_H \\ &= \overline{\epsilon} \int_{r_0}^{r_1} dr \cdot j_p(E_{ENA}) \sigma_{ex}(v_{ENA}) n_H, \end{aligned} \tag{10}$$

or

$$\overline{\epsilon} = \frac{\int_{r_0}^{r_1} dr \cdot j_p(E_{ENA}) \epsilon(\phi, \theta, r) \sigma_{ex}(v_{ENA})}{\int_{r_0}^{r_1} dr \cdot j_p(E_{ENA}) \sigma_{ex}(v_{ENA})}. \tag{11}$$

This expression strongly depends on the streamline profile due to a frame-of-reference transformation, where the curved streamlines result in different regions of the phase space of $j_p(E_{ENA})$ being sampled along a line-of-sight. In addition, the integral

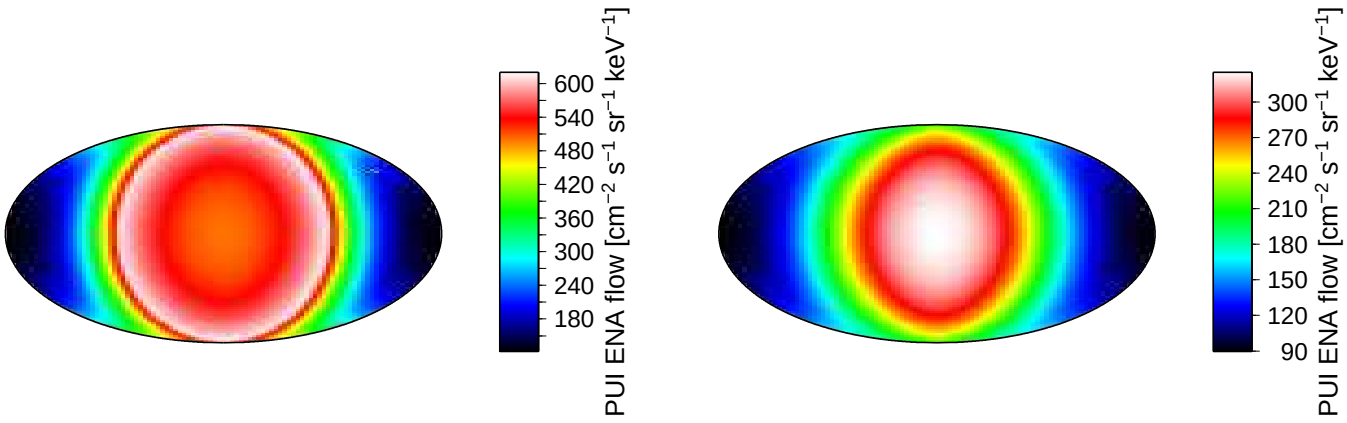

(a) $\varepsilon = 0.25$, no depletion correction

(b) $\varepsilon = 0.25$

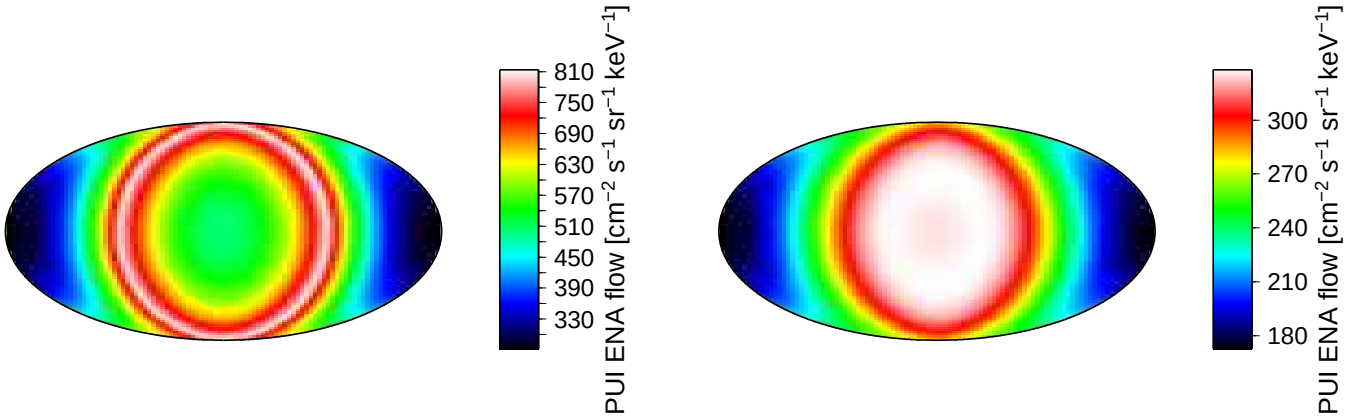

(c) $\varepsilon = 0.15$, no depletion correction

(d) $\varepsilon = 0.15$

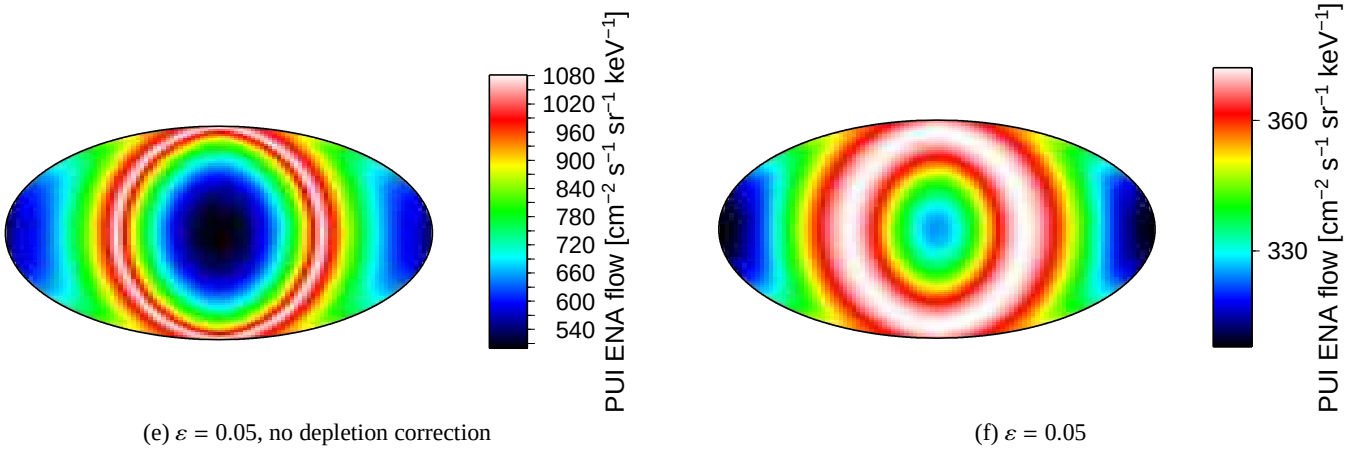

(e) $\varepsilon = 0.05$, no depletion correction

(f) $\varepsilon = 0.05$

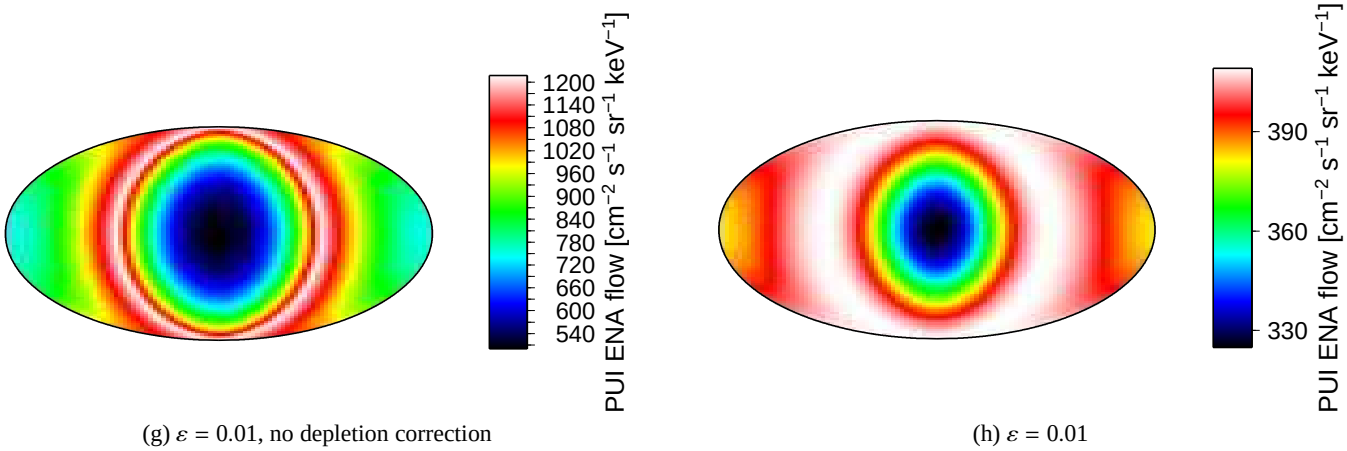

(g) $\varepsilon = 0.01$, no depletion correction

(h) $\varepsilon = 0.01$

Fig. 2: ENA flow skymaps at E_{obs} = 1 keV for different TS geometries and the presence/absence of the depletion correction.

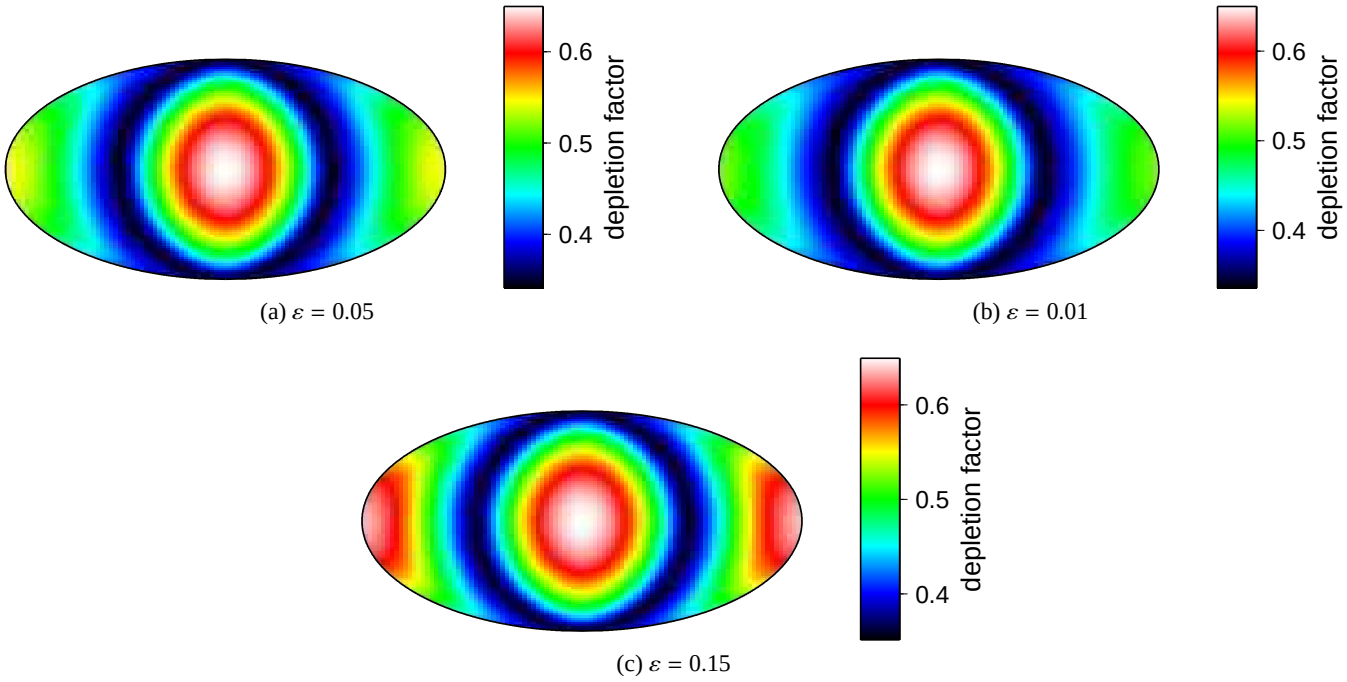

(a) $\varepsilon = 0.05$ (b) $\varepsilon = 0.01$

(c) $\varepsilon = 0.15$

Fig. 3: ENA depletion maps of the averaged depletion factor $\bar{\epsilon}$ at $E_{obs} = 1$ keV for different TS geometries. Note that small factors correspond to a large modification and vice versa.

also samples multiple different plasma flowlines, which might be characterized by qualitatively and quantitatively different source proton distribution functions. Therefore, the extinction profile calculated with the help of Eq. 11 strongly depends on model assumptions in the inner heliosheath, which offers an attractive method to verify or disprove existing numerical and analytical models of this region.

To demonstrate this behaviour, we present extinction maps for a few selected configurations in Fig. 3. In these figures, we have adopted a source distribution function following a power law of the form v^{-5}, with a constant number density on the near downstream side of the termination shock. These figures easily demonstrate that the general shape of the depletion map is almost independent on the geometry of the outer heliosphere, and that the difference in the ENA skymaps presented on Fig. 2 is primarily due to a suppression of the ENA emission feature that appears in the extinctionless skymaps. However, the extinction effect is slight weaker than the emission feature, which allows the ring feature to persist in a certain range of geometric parameters.

One additional point worth mentioning is the extinction factor in the heliotail region, where a more significant modification of the depletion factor is observed, ranging between $0.55 \leq \bar{\epsilon} \leq 0.65$ for the presented range of geometry parameters. This result suggests that the depletion mechanism might provide an additional insight in studies of the shape of the heliotail, a region that has recently found renewed interest in the IBEX community (McComas et al. 2013).

4. The depletion correction above 10 keV

In this section, we present first calculations for the depletion correction at higher energies. INCA/CASSINI observes ENA fluxes in the energy intervall between 5 and 50 keV, while the upcoming IMAP mission (the follower to the IBEX mission) is supposed to even include a detector for ENAs until up to 100 keV, and therefore we now study the depletion correction in the energy range between 10 and 100 keV.

At these higher energies, the product $v_{rel} \cdot \sigma_{ex}$ starts to drop due to the behaviour of the charge exchange cross section (see e.g. Lindsay & Stebbings 2005), resulting in a weaker depletion effect, while at the same time, the source distribution function is assumed to drop like $f(v) \propto v^{-4...-5}$ (Fahr et al. 2009), resulting in much weaker global ENA fluxes. On Fig. 4, we present depletion factors at higher energies, demonstrating that the general form of the depletion map is nearly unchanged, with only the absolute values of $\bar{\epsilon}$ being modified systematically towards higher values, i.e. a weaker depletion effect. This behaviour demonstrates that the overall form of the plasma flowline profile is well reflected by the depletion correction at all energies relevant for ENA observations, almost independent of the energy range in question.

One interesting trend that emerges in Fig. 4 is that, towards higher energies, the strongest depletion effect that is primarily found in the flanks of the heliosphere exhibits a slightly different behaviour than the depletion in the upwind (nose) and downwind (tail) directions, with the depletion growing slightly stronger with increasing energies. This is an effect of the streamline orientation; in the flanks, most streamlines sampled by the line-of-sight integral are almost perpendicular to said line-of-sight, and therefore, the velocity transformations discussed earlier result in a different relative velocity between the energetic ions and the cold interstellar hydrogen that is used to determine the charge exchange cross section.

5. Conclusions

The source depletion process identified by Siewert et al. (2014) introduces a new and significant aspect to the interpretation of IBEX ENA data, which we have now quantified for the first

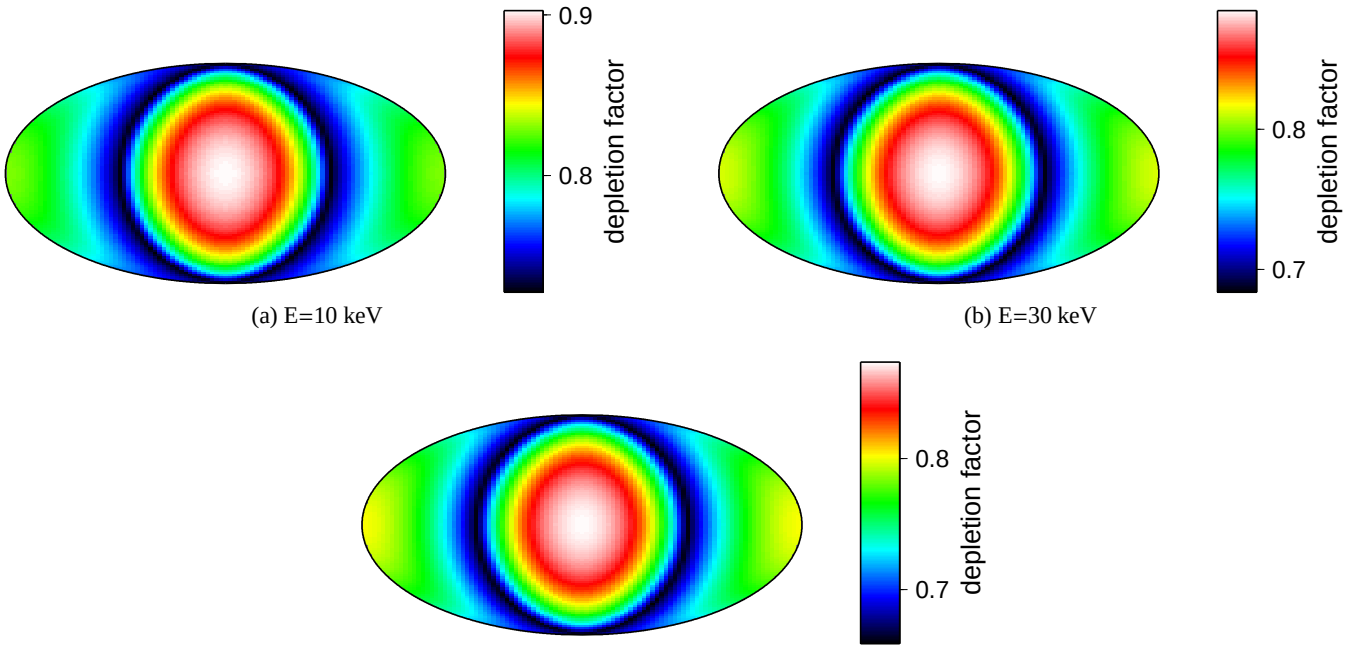

(a) E=10 keV

(b) E=30 keV

(c) E=50 keV

Fig. 4: ENA depletion maps of the averaged depletion factor $\bar{\epsilon}$ for a numerical eccentricity of $\varepsilon = 0.05$ for 10, 30 and 50 keV protons. Note that small factors correspond to a large modification and vice versa.

time. As we have demonstrated, understanding the plasma flowline profile in the inner heliosheath is critcal for understanding an inner heliosheath ENA source, as the resulting depletion factors along the line-of-sight do significantly modify the integrated ENA fluxes.

For this reason, we conclude that a realistic description of the inner heliosheath is clearly required for a full data analysis. Unfortunately, this task is greatly complicated by the very unclear observational data taken by the Voyagers, which suggests that the heliopause, i.e. the distant boundary of the heliosheath, is a very nonideal structure dominated by a combination of mostly misunderstood microphysics. Because of this, there is no clear hint towards which of the various models of the heliospheric boundary found in the literature would be the most realistic approximation; in fact, it is probable that our adopted model of this region of the heliosphere requires a major revision.

Nevertheless, our results clearly prove that the geometry and the flowline profile of the outer heliosphere leaves a strong imprint on the observed ENA skymaps, that is almost independent of the ENA energies in question. Therefore, understanding the outer heliosphere and the source depletion effect is of high importance for understanding ENAs generated in this region. Using the same arguments, it should be possible to differentiate between competing models for the outer heliosphere by calculating the characteristic depletion skymap ($\bar{\epsilon}$) in a way similar to the one we have presented here. Finally, our results demonstrate that the depletion effect is globally weaker in the energy range between 10 and 100 keV, allowing the resulting ENA fluxes to increase by a factor of 2 compared to fluxes at 1 keV. This doubles the ENA fluxes to be expected above 10 kev, which suggests that the ENA fluxes observed at higher energies by INCA/CASSINI and the upcoming IMAP mission should be higher than expected from a simple extrapolation of energetic ion spectra, resulting in a harder spectrum at the highest energies.

Acknowledgements. M. Siewert is grateful to the Deutsche Forschungsgemeinschaft for financial support granted to him in the frame of the project Si-1550/2-2.

References

Fahr, H., Chashei, I. V., & Verscharen, D. 2009, A&A, 505, 329
Fahr, H.-J. & Fichtner, H. 1991, Space Sci. Rev., 58, 193
Fahr, H.-J., Siewert, M., McComas, D. J., & Schwadron, N. A. 2011, A&A, 531, A77
Fisk, L. A. 2005, Science, 309, 2016
Heerikhuisen, J., Pogorelov, N. V., Florinski, V., Zank, G. P., & le Roux, J. A. 2008, ApJ, 682, 679
Jokipii, J. R. 2008, Nature, 454, 38
Krimigis, S. M., Mitchell, D. G., Roelof, E. C., Hsieh, K. C., & McComas, D. J. 2009, Science, 1181079, http://www.sciencemag.org/cgi/content/abstract/1181079v1
Lee, M. A., Fahr, H. J., Kucharek, H., et al. 2009, Space Science Reviews, 146, 275
Lindsay, B. G. & Stebbings, R. F. 2005, Journal of Geophysical Research (Space Physics), 110, 12213
McComas, D. J., Alexashov, D., Bzowski, M., et al. 2012a, Science, 336, 1291
McComas, D. J., Allegrini, F., Bochsler, P., et al. 2009, Science, 326, 959
McComas, D. J., Dayeh, M. A., Allegrini, F., et al. 2012b, ApJS, 203, 1
McComas, D. J., Dayeh, M. A., Funsten, H. O., Livadiotis, G., & Schwadron, N. A. 2013, ApJ, 771, 77
McComas, D. J., Lewis, W. S., & Schwadron, N. A. 2014, Rev. Geophys., 52, 118
Scherer, K. & Fahr, H. 2009, A&A, 495, 631
Siewert, M., Fahr, H.-J., & McComas, D. J. 2014, A&A, 565, A81
Siewert, M., Fahr, H.-J., McComas, D. J., & Schwadron, N. A. 2012, A&A, 539, A75
Siewert, M., Fahr, H.-J., McComas, D. J., & Schwadron, N. A. 2013, A&A, 551, A58
Webber, W. R. & McDonald, F. B. 2013, Geophys. Res. Lett., 40, 1665